Multi-level analysis of the northern polar vortex split in April 2020 during development of the Arctic ozone hole

Jezabel Curbelo[1], Gang Chen[2], and Carlos Roberto Mechoso[2]

[1]Universitat Politècnica de Catalunya
[2]University of California Los Angeles

November 30, 2022

Abstract

The present paper examines the northern stratosphere during April 2020, when the polar vortex split into two cyclonic vortices. We examine this split at middle as well as lower stratospheric levels, and the interactions that occurred between the resulting two vortices which determined the distribution of ozone among them. We also examine the connections among stratospheric and tropospheric events during the period. For analysis, we apply Lagrangian tools and an Eulerian diagnostic of planetary wave activity. Our findings confirm the key role for the split played by a flow configuration with a polar hyperbolic trajectory and associated manifolds. A trajectory analysis illustrates the transport of ozone between the vortices during the split. We argue that these stratospheric events were linked to strong synoptic scale disturbances in the troposphere forming a wave train from the north Pacific to North America and Eurasia.

Multi-level analysis of the northern polar vortex split in April 2020 during development of the Arctic ozone hole

J. Curbelo[1], G. Chen[2], and C. R. Mechoso[2]

[1]Departament de Matemàtiques, Universitat Politècnica de Catalunya, Barcelona, Spain
[2]Department of Atmospheric and Oceanic Sciences, University of California, Los Angeles, CA, USA

Key Points:

- Lagrangian structures play a key role in the flow evolution leading to the vortex split.
- The split was linked to strong synoptic scale disturbances in the troposphere.
- Approach based on a Lagrangian analysis of the regional flow evolution.

Corresponding author: Jezabel Curbelo, `jezabel.curbelo@upc.edu`

Abstract

The present paper examines the northern stratosphere during April 2020, when the polar vortex split into two cyclonic vortices. We examine this split at middle as well as lower stratospheric levels, and the interactions that occurred between the resulting two vortices which determined the distribution of ozone among them. We also examine the connections among stratospheric and tropospheric events during the period. For analysis, we apply Lagrangian tools and an Eulerian diagnostic of planetary wave activity. Our findings confirm the key role for the split played by a flow configuration with a polar hyperbolic trajectory and associated manifolds. A trajectory analysis illustrates the transport of ozone between the vortices during the split. We argue that these stratospheric events were linked to strong synoptic scale disturbances in the troposphere forming a wave train from the north Pacific to North America and Eurasia.

Plain Language Summary

The evolution of the Northern Hemisphere stratosphere during late winter and early spring of 2020 was punctuated by outstanding events both in dynamics and tracer evolution. These events ranged from an episode of polar warming at upper levels in March, a polar vortex split into two cyclonic vortices at middle and lower levels in April, and a remarkably deep and persistent mass of ozone poor air within the westerly circulation throughout the period. The latter feature was particularly remarkable during 2020, which showed the lowest values of stratospheric ozone on record. We search for the answer to several outstanding questions in stratospheric dynamics and tracer evolution: What flow structures lead to the split? How was the transfer of fluid parcels from one vortex to the other after the split? Were these events connected to tropospheric events? Our approach to answer these questions is based on following air parcels trajectories, examining barriers to the flow, and the activity and propagation of planetary waves. We highlight the special polar configuration associated with stratospheric vortex splits. Our trajectory analysis illustrates the transport of ozone between the vortices during the split. Also, the split was associated with strong perturbations in the troposphere.

1 Introduction

The Northern Hemisphere stratosphere during late winter and early spring of 2020 was remarkable in several ways. The polar night vortex was strong and persistent from December to February, while wave activity input from the troposphere was low (Lee et al., 2020) and the Arctic Oscillation was in an unprecedentedly strong positive phase (Lawrence et al., 2020; Hardiman et al., 2020). The stratosphere during winter-early spring 2020 showed the lowest values of stratospheric ozone on record (Manney et al., 2020; Wohltmann et al., 2020). Also, dramatic dynamical events occurred as the final warming proceeded. These included around mid-March a warming of the polar region in the upper stratosphere amounting to tens of Kelvins. Around mid-April, the main cyclonic vortex of the polar night was joined by another cyclonic vortex, which developed from the upper troposphere to the middle stratosphere roughly above northern North America. The two vortices remained clearly identifiable for a few days, interacting with each other although the lowest ozone mixing ratio (O_3) remained within the older one. Afterwards, the westerly circulation weakened following the seasonal evolution to summer conditions. These outstanding dynamics and tracer events raise a number of questions. What processes lead to the mid-April split of the westerly polar vortex at middle levels? What types of interactions occurred between the two resulting vortices such that the lowest O_3 values remained within one of them? Were these stratospheric events connected to tropospheric events?

The present paper focuses on the vortex split in April 2020 and associated features in the ozone distributions. The period and issues we will examine provide an ideal case for a

Lagrangian analysis of the evolving flow in the stratosphere and its connections with the troposphere. Although O_3 is not strictly a conservative quantity, it has been taken as a tracer at time scales in the order of days and hence can provide an approximate depiction of fluid parcels behavior on isentropic surfaces. Therefore, our approach for analysis will be based on the application of Lagrangian tools to the flow field. We have used such tools to study the unique vortex split event in the southern stratosphere during the final warming of 2002 (Curbelo et al., 2019b). This work included a novel definition of the polar vortex boundary and the proposal of a criterion that justifies why at an isentropic level a pinched vortex will split at later times. The paper also addresses the connections with the troposphere, for which we use a Eulerian diagnostic of wave activity and its propagation following Plumb (1985).

We start in section 2 with a description of data and methods. Section 3 is a multi-level description of the flow with an emphasis on the vortex split in the stratosphere and on the stratosphere-troposphere links. Section 4 examines the distribution of fluid parcels between the vortices resulting from the split. Section 5 discusses the connections with the troposphere. Finally, we present our conclusions in section 6 .

2 Data and methods

We use daily averages of the hourly data from ERA5, the fifth generation ECMWF atmospheric reanalysis of the global climate Copernicus Climate Change Service (C3C) (Hersbach et al., 2018). The data provides wind velocity $[ms^{-1}]$, geopotential height $[m^2s^{-2}]$, potential vorticity $[Km^2kg^{-1}s^{-1}]$ and O_3 $[kgkg^{-1}]$. The resolution of the data we analyze is 0.25° lon. × 0.25° lat. with 37 pressure levels.

Our Lagrangian descriptor of choice is the function M (Mancho et al., 2013). This is defined by the expression,

$$M(\mathbf{x}_0, t_0, \tau) = \int_{t_0-\tau}^{t_0+\tau} \|\mathbf{v}(\mathbf{x}(t;\mathbf{x}_0), t)\| \, dt \ , \tag{1}$$

where $\mathbf{v}(\mathbf{x}, t)$ is the velocity field and $\|\cdot\|$ denotes the Euclidean norm. Geometrically, a fluid parcel that is at x_0 when $t = t_0$ travels a length M during the period from $(t_0 - \tau)$ to $(t_0 + \tau)$. The calculation of M is straightforward; details are given in Curbelo et al. (2017). Numerical experimentation has shown that for sufficiently large values of τ, the locations where $\|\nabla M\|$ has large magnitudes approximate those of manifolds. These locations form three-dimensional surfaces, which can be interpreted as approximations to instantaneous flow barriers. A large part of our Lagrangian analysis will be carried out over isentropic surfaces on which manifolds appear as curves. The intersections of the curves corresponding to unstable and stable manifolds give the approximate locations of hyperbolic trajectories (HT) from (to) which parcel asymptotically approach (separate) at different times. The figures showing maps in what follows represent manifolds as curves where $\|\nabla M\| > 0.7 \max(\|\nabla M\|)$ in the discretized gradient field over the entire northern hemisphere at the time.

M also provides a visualization of the (kinematic) vortex boundary that is helpful in transport studies. Curbelo et al. (2019b) employed arguments of ergodic theory to conjecture that, on either a horizontal or an isentropic surface, a contour of M for a value very close to its maximum on the surface would be such that, (i) it divides the SPV core from its surroundings, and (ii) it is free of hyperbolic trajectories and hence tends to not produce filaments during a certain time interval. In a nutshell, regions with large values of M computed with sufficiently large values of τ represent barriers of the flow. On the basis of results from numerical experiments Curbelo et al. (2019b) suggested that the threshold for M normalized by its maximum at each level can be taken as the lower limit of the fat tail in its probability density function (PDF). In the present paper we define the kinematic vortex boundary as the region where the normalized value of M at each level is larger than 0.93.

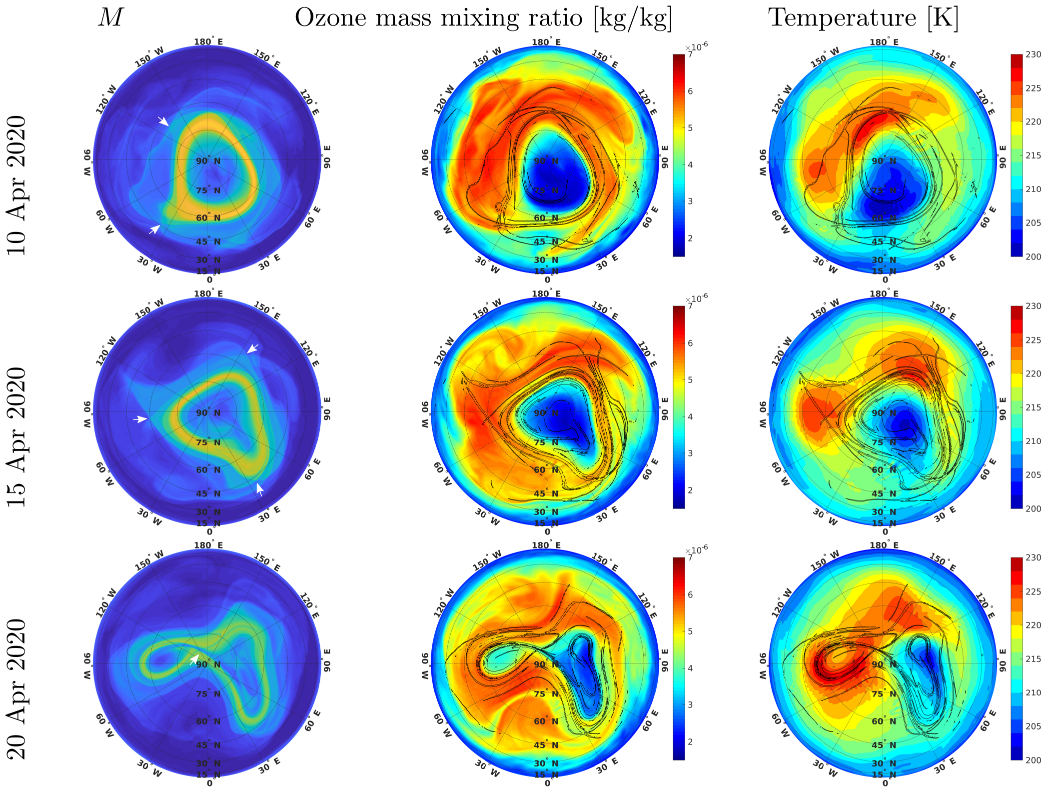

Figure 1. Horizontal section at 50hPa of the Lagrangian descriptor M, ozone mass mixing ratio [kg/kg] and temperature [K] from several days in April 2020. The black lines highlight singular features of the function M, and corresponds to large values of $\|\nabla M\|$ as defined in the text. HT are indicated with white arrows.

Note that according to this definition, the vortex boundary becomes a three-dimensional region contained between one inner and one outer surface instead of the single surface defined by the usual criterion based on potential vorticity and its maximum gradient in latitude.

3 The vortex split in April 2020

Figure 1 shows snapshots in the middle stratosphere of M, O_3, and temperature at 50 hPa. The yellowish colors in M identify parcels moving with high velocities having larger displacements; bluish zones corresponding to lower velocities and shorter trajectories. The deep blue colors in the O_3 plots are for the smaller values, while the red colors are for the larger values. Red colors in the right column of the figure are for higher temperatures and blue colors for the lower ones.

The plots on 10 April show a well-defined vortex primarily symmetric about the North Pole. There is evidence of an anticyclonic circulation over the North Atlantic and of an HT around $(45°W, 40°N)$. Inspection of the Hovmöller diagrams for longest planetary waves at 50 hPa (Fig. S1) show that the latitude of this HT corresponds to the critical level for wave 1, which is traveling eastward at the time. The unstable manifold extends west from this HT and has a clear signature on the large O_3 values over North America. Although it is less sharply defined, there is another HT near the outer periphery of the vortex at around $(130°W, 65°N)$. This HT is around the critical level for wave 2, which is also traveling eastward at the time. From this HT, a plume of large O_3 values extends over the northern

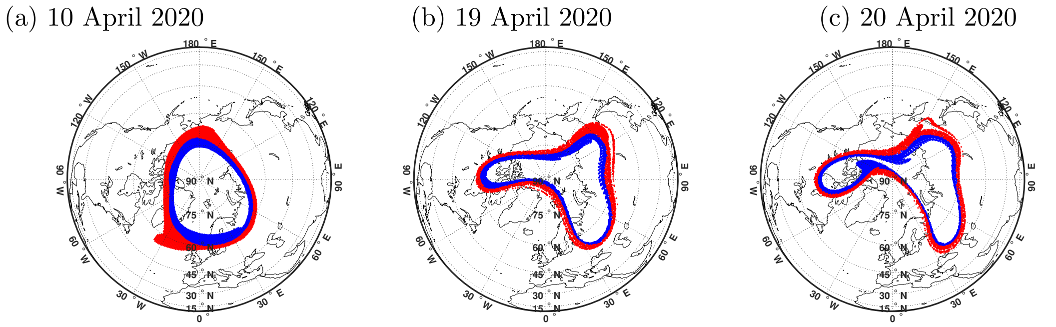

Figure 2. Locations at 50hPa of the particles selected in panel (a) for 10 April 2020 at different times of the SPV splitting. All selected particles are between the contourlines corresponding to the 93th percentile of M for 10 April 2020. The particles are drawn in either blue or red to differentiate those that are inside or outside the contour defined by the maximum value of M at each longitude.

Pacific. The O_3 plots also show how the manifolds enclose the region of very low values inside the vortex. The relationship between manifolds and temperatures is less direct, however, as temperature is not a conservative property. Nevertheless, larger O_3 values and warmer temperatures are found over northern North America and Pacific Ocean. The plots on 15 April are more complex. According to M, the vortex is still around the pole but its shape is more triangular as zonal wavenumber 3 has amplified (Fig. S1). The HTs detected on April 10 have rotated eastward and another one can be discerned around $(140°E, 50°N)$. The imprints of the HTs on O_3 and temperature are clearly visible in the plots of these quantities. The plots change dramatically from 15 to 20 April: another HT has developed very near the pole in association with the amplification of zonal wavenumber 2 (see Fig. S1).

The configuration of the manifolds associated with the polar HT plays key roles in the vortex split (see Fig. S2). To see the importance of such configuration, we look jointly at the plots of M and the manifolds for 20 April in Fig. 1. Fluid parcels traveling at higher speeds - as evidenced by the larger values of M - from the periphery of the vortex in the eastern hemisphere to the periphery of the vortex in the western hemisphere first approach the polar hyperbolic point along the stable manifold and next move away from it along the unstable manifold. As the parcels return to the eastern hemisphere, their path to the polar hyperbolic point is obstructed by the manifolds that have formed ahead. For a while, some of the parcels keep circling around the vortex in the western hemisphere while others are able to reach the other vortex. At some point in time the latter transfer is interrupted and the two vortices split.

The behaviors described in the previous paragraph are illustrated by parcel trajectories in Fig. 2. In this figure, trajectories are computed forward in time as in Curbelo et al. (2019a). For visualization, particles within the vortex boundary are colored either blue or red according to whether they are in the equatorward or poleward the contour of max(M) at the selected level. Recall that the vortex boundary is defined by the contours where the value of M is in the upper 7%. On 19 April the colored parcels surround the vortex, which is already considerably deformed. One day later, on 20 April, some of the blue parcels are returning over northern North America to the western hemisphere vortex, in a configuration that strongly resembles the schematics in Fig. S2 while others still continue to the other vortex. The vortex split is completed one day later (not shown).

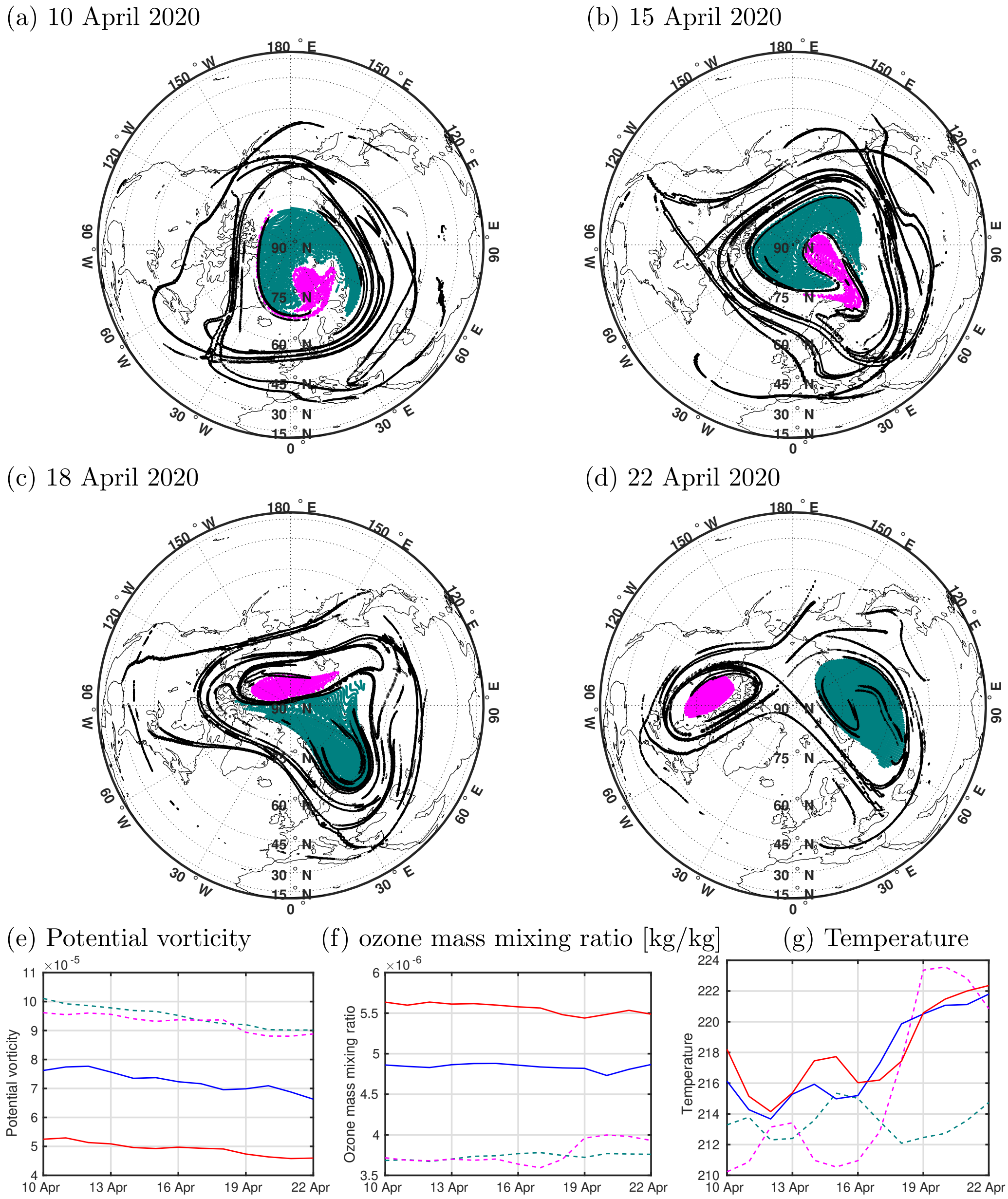

Figure 3. Panels (a)-(d) display backward parcel trajectories at 530K. In the panels, black lines correspond to large values of $\|\nabla M\|$, i.e. approximate the manifolds. Magenta color identifies parcels that on 22 April have O_3 values both in the lower 4% and above the lower 1.5% for the level. Green color identifies parcels on 22 April have O_3 values in the lower 4% for the level. Panels (e)-(g) show the time series of mean potential vorticity, ozone mass mixing ratio, and temperature for the sets of particles in green and magenta, as well as for those in red and blue in Fig. 2. See the text for more information.

4 Transfer of fluid parcels between the vortices during and after the split

In this section we look into how the transfer of fluid parcels between vortices occurred at 530K, and to what extent O_3 behaved as an inert tracer. To answer the first question, we plot backward trajectories starting on 22 April of selected parcels inside the vortices over

North America and northern Eurasia. Panels (a)-(d) of Fig. 3 show in magenta color the locations at different times of parcels starting in the western hemisphere and characterized by O_3 values both in the lower 4% and above the lower 1.5% for the level. Green color identifies parcels that on 22 April are in the eastern hemisphere and have O_3 values in the lower 4% for the level and thus includes the lowest ozone concentrations. On 18 April, the set of parcels labeled with magenta color is very near the North Pole at both sides of the dateline. On 15 April, these parcels are over Eurasia inside a U-shaped pattern formed by those labeled with green color. On 10 April, the configuration is very similar to the one 5 days later. The panels of Fig. 3 reveal that a set of parcels well within the vortex core on 10 April move clockwise around the pole and along its inner boundary until they are transferred to the new vortex in the western hemisphere. The panels also reveal that parcels with the lowest O_3 values on April 22 did not transfer from the vortex over north Eurasia to that over North America. Movie S4 illustrates these parcels displacements with higher temporal resolution

Panels (e), (f) and (g) of Fig. 3 show the time evolution of mean potential vorticity, O_3 and temperature respectively, for the different sets of particles represented in panels (a)-(d) of the same figure (green and magenta lines) and in Fig. 2 (blue and red lines). The time series of potential vorticity shows a slightly decreasing trend. The values of O_3 (Fig. 3(f)) are relatively constant with a slight decreasing trend before April 20. The lowest ozone values are inside the vortex in the outer part (red line) of the vortex boundary is larger than in the inner part (blue line). This is in general agreement with the presence of an "ozone collar" around the vortex as reported by Mariotti et al. (2000) for the Antarctic polar vortex on the basis of airplane data. Fig. 3(g) shows a different behavior for temperature, without clear separations between the different colored regions. Note the temperature increase captured by the magenta line from 17 to 19 April, at which time the green line captures a decrease. These temperature variations broadly agree with those expected from the split shown in the panels of Fig. 1.

5 Connections with the troposphere

The outstanding feature in the troposphere of the Northern Hemisphere during April 2020 was a strong ridge south of Alaska. A trough downstream of that ridge was associated with a significant cold air event for mid-western U.S. This configuration is associated with a negative East Pacific Oscillation (EPO). In mid-April 2020, the configuration at high latitudes was also consistent with a positive Pacific-North American (PNA) pattern suggesting a tropical influence as sea surface temperatures in the eastern equatorial Pacific were warmer than average by about 0.5 K during fall 2019 and winter 2020. To explore whether these extreme events were linked to the stratosphere we use the Eulerian diagnostics of wave activity flux F defined in equation (5.7) of Plumb (1985).

Figure 4(a) shows the horizontal component of F (Plumb, 1985) for 15 April 2020 at 250hPa; in this figure colors correspond to values of the vertical component of F. A wave train spanning from the center of large upward vertical flux around $(180°W, 50°N)$ is clearly observed in the QG stream function. Another region of large upward vertical flux is centered around $(75°W, 60°N)$. The largest downward flux is at around $(50°E, 60°N)$. For a closer look at the wave activity flux field, figure 4 shows vertical cross-sections of F averaged in the latitude band $55°N - 65°N$ for 15 (b), 20 (c) and 25 of April (d), i.e at the vortex pinching, vortex split, and after the two vortices have formed. The contours in the panels are the deviation of the QG stream function from the zonal mean. On 15 April, the negative stream function anomaly in panel (b) represents a cyclonic circulation centered over North America around $75°W$ extended up to 100hPa. At the center of this circulation, the wave activity flux was upward as also seen in panel (a). After 5 days, this anomaly reached levels above 10hPa, where the wave activity flux is strong and upward (see also Fig. 2). The other circulations associated with the wavetrain mentioned before are evident in panel (b). Another feature seen in panel (b) at upper levels is the vortex over northern Eurasia

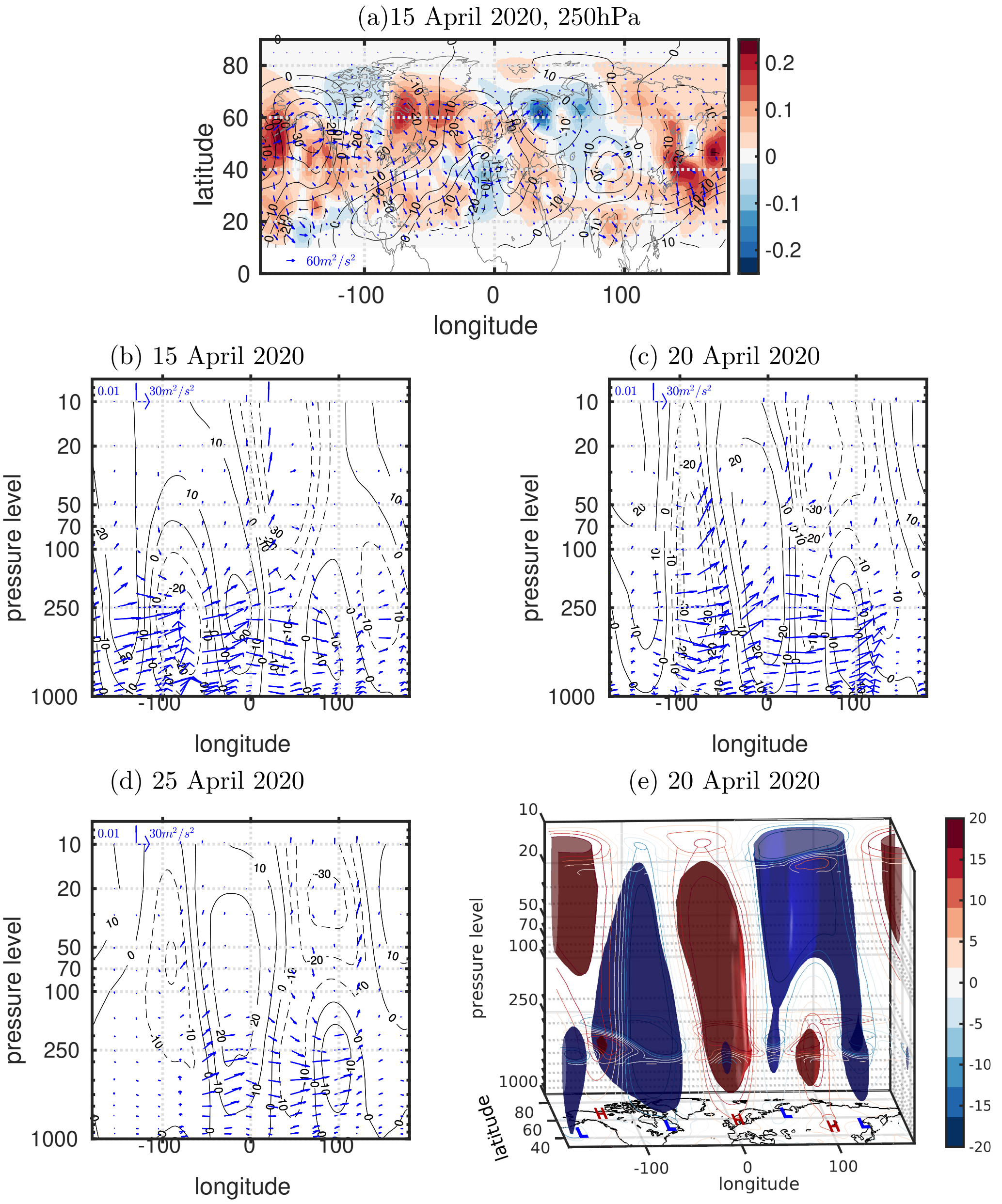

Figure 4. (a) Horizontal component of wave-activity flux F (Plumb, 1985) for 15 April at 250 hPa. The color in this panel corresponds to the vertical component of F. (b), (c), and (d) Vertical cross-section of F averaged between $55°N$-$65°N$ for 15, 20 and 25 April, respectively. Contours are for positive (solid) and negative (dashed) deviations of QG stream function from the zonal mean (contour interval $10km^2/s$). (e) Isosurfaces of deviations of QG stream function from the zonal mean at values of -15km^2/s (blue) and 20km^2/s(red). For added clarity, contour lines are drawn on the pressure surfaces at 1000hPa, 250hPa and 10hPa, as well as on the vertical surface at $65°N$.

where the vertical wave activity flux is upward. Notice that at low level under this vortex the vertical wave activity flux is downward. One more feature of interest in panel (b) is the downward vertical wave activity flux into the anticyclonic circulation centered around $100°E$. The patterns on 20 April shown in panel (c) are essentially and amplification of those 5 days earlier. On 25 April, panel (d) shows the signature of zonal wavenumber 2 at upper levels, while the component of the tropospheric wavetrain below 100 hPa is still visible especially in the eastern hemisphere. These configurations of vertical wave activity flux suggests stratosphere-troposphere connections that were several kilometers deep. See also longitude - height sections of M, O_3 and manifolds in Fig. S3. After the vortex split, on 25 April (panel (d)), the vertical wave activity flux decays in magnitude around $90°W$. Notably, F pointed slightly downward in the eastern hemisphere around $90°E$ suggests that the stratosphere is influencing the troposphere over northern Eurasia at this time as in the connections discussed by Kretschmer et al. (2018). The vortex over North America has a clearly defined troposphere-stratosphere structure, decreasing its size in height and closing at 30hPa. Conversely, the vortex over Eurasia is better defined in the stratosphere. Figure 4 (e) shows the isosurfaces of the QG stream function anomaly at value of -15km^2/s (blue) and 20km^2/s (red). Contour lines on the pressure surfaces at levels 1000hPa, 250hPa and 10hPa, as well as on the vertical surface at $65°N$, are shown in the same panel to give an idea of the more complete vertical structure of the circulations.

6 Conclusions

We have examined dynamics and tracer events occurring in the northern stratosphere around mid-April, when the main cyclonic vortex of the polar night displaced oner northern Eurasia was joined by another cyclonic vortex that developed above northern North America. The two vortices remained distinct for a few days, after which they merged until the final warming was completed in mid-May. Our emphasis was placed on the split of the westerly polar vortex at middle levels and on the interactions that occurred between the two vortices determining the resulting distribution of ozone. Emphasis was also placed on the connections among stratospheric and tropospheric events during the period. For the analysis we applied Lagrangian tools, including the estimation of HTs and associated manifolds as well as a novel definition of the polar vortex boundary. We also used a Eulerian diagnostic of planetary wave activity and its propagation.

Inspection of the flow evolution prior to the vortex split revealed a configuration in which a polar hyperbolic trajectory (HT) plays a key role. Fluid parcels from the periphery of the vortex in the eastern hemisphere traveling at higher speeds towards near the HT along its stable manifold continue moving along the periphery of the vortex in the western hemisphere along the unstable manifold. As some of these parcels return to the eastern hemisphere, their path is obstructed by other developing manifolds and stay circling around the vortex in the western hemisphere while others are able to reach the other vortex. At some point in time, these transfer were interrupted and the two vortices split. Such a behavior is similar to the one described in the vortex split during the final warming of the southern stratosphere during spring of 2002 (Curbelo et al., 2019b).

The evolutions described in the previous paragraph were illustrated by the field of parcel trajectories. Examination of this field further revealed that a set of parcels well within the vortex core on 10 April moved clockwise around the pole and along its inner boundary until it transferred to the new vortex in the western hemisphere. Thus, the lower values of ozone were in the vortex interior over Eurasia on 22 April.

During mid-April 2020, a strong ridge set in the northeastern Pacific accompanied downstream over northern North America by a similarly strong trough; there were also wave-like features both upstream and downstream of the ridge-trough pair. Such a configuration is consistent with the excitation of well-know patterns of northern hemisphere winter variability that might even include tropical-extratropical connections because sea surface temperatures in the eastern equatorial Pacific were warmer than average during the period. The strong trough developed vertically resulting in a close circulation in the middle and lower stratosphere. Horizontal energy transfers are consistent with an amplification of a ridge pattern over the North Atlantic. This ridge, in turn, extended vertically to the middle stratosphere. The pattern continued a downstream development, in which the downward pointing wave-activity flux suggests stratospheric influences on the troposphere over northern Eurasia.

Connections with the troposphere in the events leading to the vortex split just described were also found during the final warming of the southern stratosphere in 2002 (Curbelo et al., 2019a), including possible teleconnections with the tropics (Nishii & Nakamura, 2004). The vortex split in the the southern stratosphere, however, resulted in two vortices of comparable strength and extent suggesting that amplification of zonal wavenumber 2 was an important dynamical contributor. From this viewpoint, Esler et al. (2006) posited that the Antarctic stratospheric sudden warming of 2002 resulted from a self-tuned resonance involving nonlinear feedbacks. The vortices produced after the split described in the present paper were substantially different from each other, and although the amplitude of zonal wave number 2 also increased the contribution of other wavenumbers was relatively higher. Numerical experiments have suggested that tropospheric precursors play a major role in the stratospheric warming events except for stratospheric preconditioning very close to the onset date (Sun et al., 2012). We interpret these arguments as supportive of close links between tropospheric and stratosphere during mid April 2020, rather than an *in situ* instability.

Acknowledgments

Support was provided by the U.S. NSF Grant AGS-1832842. J.C. also acknowledges the support of the RyC project RYC2018-025169.

Data Availability Statement: The data sets used here are publicly available: ERA5, Copernicus Climate Change Service (C3S) operated by ECMWF on behalf of the European Commission. DOI: 10.24381/cds.bd0915c6. They were obtained from `https://cds.climate.copernicus.eu/cdsapp#!/dataset/reanalysis-era5-pressure-levels?tab=form` [registration required]

References

Curbelo, J., García-Garrido, V. J., Mechoso, C. R., Mancho, A. M., Wiggins, S., & Niang, C. (2017). Insights into the three-dimensional lagrangian geometry of the antarctic polar vortex. *Nonlinear Processes in Geophysics*, *24*(3), 379–392.

Curbelo, J., Mechoso, C., Mancho, A. M., & Wiggins, S. (2019a). Lagrangian study of the final warming in the southern stratosphere during 2002: Part II. 3D structure. *Climate Dynamics*, *53*(3-4), 1277–1286.

Curbelo, J., Mechoso, C., Mancho, A. M., & Wiggins, S. (2019b). Lagrangian study of the final warming in the southern stratosphere during 2002: Part I. the vortex splitting at upper levels. *Climate Dynamics*, *53*(5-6), 2779–2792.

Esler, J. G., Polvani, L. M., & Scott, R. K. (2006). The antarctic stratospheric sudden warming of 2002: A self-tuned resonance? *Geophysical Research Letters*, *33*(12), L12804.

Hardiman, S. C., Dunstone, N. J., Scaife, A. A., Smith, D. M., Knight, J. R., Davies, P., ... Greatbatch, R. J. (2020). Predictability of european winter 2019/20: Indian ocean dipole impacts on the nao. *Atmospheric Science Letters*, *21*(12), e1005.

Hersbach, H., Bell, B., Berrisford, P., Biavati, G., Hornyi, A., Muoz Sabater, J., ... Thpaut, J.-N. (2018). ERA5 hourly data on pressure levels from 1979 to present. *Copernicus Climate Change Service (C3S) Climate Data Store (CDS). (Accessed on 10-Nov-2020).* Retrieved from `10.24381/cds.bd0915c6`

Kretschmer, M., Cohen, J., Matthias, V., Runge, J., & Coumou, D. (2018). The different stratospheric influence on cold-extremes in eurasia and north america. *npj Clim Atmos Sci*, *1*(44).

Lawrence, Z. D., Perlwitz, J., Butler, A. H., Manney, G. L., Newman, P. A., Lee, S. H.,

& Nash, E. R. (2020). The remarkably strong arctic stratospheric polar vortex of winter 2020: Links to record-breaking arctic oscillation and ozone loss. *Journal of Geophysical Research: Atmospheres*, *125*(22), e2020JD033271.

Lee, S. H., Lawrence, Z. D., Butler, A. H., & Karpechko, A. Y. (2020). Seasonal forecasts of the exceptional northern hemisphere winter of 2020. *Geophysical Research Letters*, *47*(21), e2020GL090328.

Mancho, A. M., Wiggins, S., Curbelo, J., & Mendoza, C. (2013). Lagrangian descriptors: A method for revealing phase space structures of general time dependent dynamical systems. *Communications in Nonlinear Science and Numerical Simulations*, *18*(12), 3530-3557.

Manney, G. L., Livesey, N. J., Santee, M. L., Froidevaux, L., Lambert, A., Lawrence, Z. D., ... Fuller, R. A. (2020). Record-low arctic stratospheric ozone in 2020: Mls observations of chemical processes and comparisons with previous extreme winters. *Geophysical Research Letters*, *47*(16), e2020GL089063. doi: https://doi.org/10.1029/2020GL089063

Mariotti, A., Mechoso, C. R., Legras, B., & Daniel, V. (2000). The Evolution of the Ozone Collar in the Antarctic Lower Stratosphere during Early August 1994. *Journal of the Atmospheric Sciences*, *57*(3), 402-414.

Nishii, K., & Nakamura, H. (2004). Tropospheric influence on the diminished antarctic ozone hole in september 2002. *Geophysical Research Letters*, *31*, L16103.

Plumb, R. A. (1985). On the Three-Dimensional Propagation of Stationary Waves. *Journal of the Atmospheric Sciences*, *42*(3), 217-229.

Sun, L., Robinson, W. A., & Chen, G. (2012). The Predictability of Stratospheric Warming Events: More from the Troposphere or the Stratosphere? *Journal of the Atmospheric Sciences*, *69*(2), 768-783. doi: 10.1175/JAS-D-11-0144.1

Wohltmann, I., von der Gathen, P., Lehmann, R., Maturilli, M., Deckelmann, H., Manney, G. L., ... Rex, M. (2020). Near-complete local reduction of arctic stratospheric ozone by severe chemical loss in spring 2020. *Geophysical Research Letters*, *47*(20), e2020GL089547. doi: https://doi.org/10.1029/2020GL089547